Accepted Manuscript

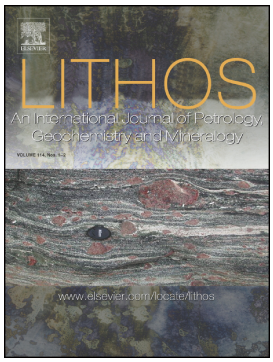

A common parentage - Low abundance trace element data of gem diamonds reveals similar fluids to fibrous diamonds

M.Y. Krebs, D.G. Pearson, T. Stachel, F. Laiginhas, S. Woodland, I. Chinn, J. Kong

PII: S0024-4937(18)30450-X
DOI: https://doi.org/10.1016/j.lithos.2018.11.025
Reference: LITHOS 4879

To appear in: *LITHOS*

Received date: 19 July 2018
Accepted date: 20 November 2018

Please cite this article as: M.Y. Krebs, D.G. Pearson, T. Stachel, F. Laiginhas, S. Woodland, I. Chinn, J. Kong , A common parentage - Low abundance trace element data of gem diamonds reveals similar fluids to fibrous diamonds. Lithos (2018), https://doi.org/10.1016/j.lithos.2018.11.025

A common parentage - Low abundance trace element data of gem diamonds reveals similar fluids to fibrous diamonds

M. Y. Krebs[1,*] mkrebs@gia.edu, D. G. Pearson[1], T. Stachel[1,2], F. Laiginhas[3], S. Woodland[1], I. Chinn[4] & J. Kong[5]

[1]Department of Earth and Atmospheric Sciences, University of Alberta, Edmonton, Canada

[2]Canadian Centre for Isotopic Microanalysis, University of Alberta, Edmonton, Canada

[3]Department of Earth Sciences, Durham University, U.K

[4]De Beers Group Exploration, South Africa

[5]De Beers Canada

[*]Corresponding author at: Gemological Institute of America, 4th Floor, 50 West 47th Street, 10036 New York, NY, USA.

Abstract

Quantitative trace element data from high-purity gem diamonds from the Victor Mine, Ontario, Canada as well as near-gem diamonds from peridotite and eclogite xenoliths from the Finsch and Newlands mines, South Africa, acquired using an off-line laser ablation method show that we see the same spectrum of fluids in both high-purity gem and near-gem diamonds that was previously documented in fibrous diamonds. "Planed" and "ribbed" trace element patterns characterize not only the high-density fluid (HDF) inclusions in fibrous diamonds but also in gem diamonds. Two diamonds from two Finsch harzburgite xenoliths show trace element patterns similar to those of saline fluids, documenting the involvement of saline fluids in the precipitation of gem diamonds, further strengthening the link between the parental fluids of both gem and fibrous diamonds. Differences in trace element characteristics are evident between Victor diamonds containing silicate inclusions compared with Victor diamonds containing sulphide inclusions. The sulphide-bearing diamonds show lower levels of inter-element fractionation and more widely varying siderophile element concentrations - indicating that the silicate and sulphide-bearing diamonds likely formed by gradations of the same processes, via melt-rock reaction or from a subtly different fluid source. The shallow negative $LREE_N$-$HREE_N$ slopes displayed by the Victor diamonds establish a signature indicative of original derivation of the diamond forming agent during major melting (~10 % melt). Consequently, this signature must have been passed on to HDFs separating from such silicate melts.

Keywords: Trace Elements; Diamond; Laser ablation; diamond HDFs; Victor diamond mine

1. Introduction

Diamond crystallizes from a fluid/melt phase - relics of which may become trapped and, thus preserved in the form of inclusions (Navon et al., 1988). To understand the origin of diamonds it is essential to constrain the nature of these so-called high-density fluid (HDF) inclusions. Fibrous and "cloudy" diamonds trap a high number of HDF inclusions and, therefore, have been extensively studied using major and trace element compositions, resulting in the identification of four major compositional types of HDFs (saline, high-Mg and low-Mg carbonatitic, and silicic) that form two compositional arrays. One array extends between the saline and high-Mg carbonatitic end-members and a second ranges from low-Mg carbonatitic to the silicic end-member (e.g., Navon et al., 1988; Izraeli et al., 2001; Tomlinson et al., 2006; Klein-BenDavid et al., 2007; Weiss et al., 2009).

Trace element patterns of diamond HDFs have been classified into two end-members: "planed" (fairly flat and unfractionated) and "ribbed" (highly fractionated) (e.g., Tomlinson et al., 2009; Weiss et al., 2009, 2011; Klein-BenDavid et al., 2010; Smith et al., 2012). The planed patterns can be related to an asthenospheric source whereas the ribbed patterns are proposed to represent increased interaction with the sub-continental lithospheric mantle (Weiss et al., 2013).

It is important to note that while the composition of HDFs trapped inside fibrous diamond is well constrained, their exact nature and composition at the time of entrapment/diamond formation is still subject to extensive research. The general consensus is that primary HDFs are high-density fluids, highly enriched in carbon and water, whose chemical nature is similar to supercritical liquids with melt-like solubilities (Klein Ben-David et al., 2006; Weiss et al., 2010). Bureau et al. (2012) have shown experimentally that diamonds can also grow from two fluids - a hydrous silicate carbon-bearing fluid (or melt) and an aqueous fluid - in equilibrium with each other.

Fibrous diamonds typically occur as either cuboids or coated stones. Most fluid-rich fibrous and cloudy diamonds are thought to have formed within 5 My of the age of kimberlite eruption, based on low nitrogen aggregation states (e.g., Gurney et al., 2010). A recent study by Timmerman et al. (2018), however, reported minimum U-Th/He ages that suggest that some fibrous diamonds formed tens to hundreds of million years before eruption of their host kimberlite. As a consequence of this overall age relationship and the fact that the majority of known kimberlites are Phanerozoic, the study of diamond-forming fluids via fibrous diamonds may be largely limited to HDFs formed in the Phanerozoic. One known exception are the Archean fibrous Wawa diamonds studied by Smith et al. (2012). The formation of gem diamonds (here defined as clear smooth-surfaced monocrystalline diamonds) of peridotitic or eclogitic association reaches as far back as the Archean (~3.6 Ga; Pearson and Shirey, 1999; Gurney et al., 2010). Diamonds containing harzburgitic inclusions formed generally in the Paleoarchean and those with lherzolitic inclusions predominantly in the Paleoproterozoic (Westerlund et al., 2006; Smit et al., 2010; Aulbach et al., 2018) whereas the crystallization of eclogitic suite diamonds has been documented between 2900 and 650 Ma (e.g., Shirey and Richardson, 2011; Smit et al., 2016). In addition to differences in habit and growth rate between fibrous and gem diamonds (Sunagawa, 1984), the apparent discrepancy in formation ages between the two diamond types has created doubts as to the applicability of the diamond-forming HDF compositions constrained from fibrous diamonds to the formation of gem diamonds. To address this issue it is important to characterize the trace amounts of diamond-forming HDFs that may be trapped as nano-inclusions in gem diamonds.

Jablon and Navon (2016) recently discovered rare fluid nano-inclusions on twin planes in gem diamonds from Voorspoed and Venetia that showed strong similarity in major element chemistry to fluids in fibrous diamonds, suggesting common parental fluids. Further evidence of

this proposed link may be gained through measurements of trace elements in gem diamonds. Constraining the nature of diamond-forming HDFs for high purity gem-quality diamonds, however, is hampered by the extremely low concentrations of impurities that these diamonds contain. The development of a new technique – in-situ, closed-cell laser ablation (McNeill et al., 2009; Klein-BenDavid et al., 2010) – that allows the accumulation of higher volumes of analyte, improved the signal to noise ratio many times over on-line laser ablation. This development resulted in two studies reporting quantitative data on gem diamond (McNeill et al., 2009, Melton et al., 2012). Trace element systematics for gem diamonds have also been reported by Rege et al. (2010) who analysed over 400 monocrystalline diamonds from deposits worldwide, using an online LA-ICPMS technique (Rege et al., 2005). They found very strong similarities between all analysed diamonds, regardless of locality and paragenesis. However, Rege et al. (2010) did not clearly demonstrate that their measurements met rigorous criteria for being above defined limits of quantitation (LOQ) and as a consequence, these data will not be considered in any of the comparisons made here.

Here we present a comprehensive trace element dataset for HDFs in high-purity gem diamonds (trapped as invisible nano-inclusions) from the Victor Mine, Ontario, Canada, as well as for near-gem diamonds from peridotite and eclogite xenoliths from the Finsch and Newlands mines, South Africa. We document HDF compositions for these gem diamonds and evaluate their origin and similarity to HDFs included in fibrous diamonds.

2. Samples

In this study we analysed diamonds from three different locations (Table 1). The majority of samples originate from the Victor Mine, Ontario, Canada, and are ultra-pure gem-quality peridotitic diamonds in the form of polished plates. The Victor plates range between 0.23 and

0.55 carats and their paragenesis was constrained from the solid macro-inclusions they contain. Eight peridotitic garnet inclusion-bearing and eight sulphide inclusion-bearing diamonds were selected for analysis. Victor diamonds containing silicate inclusions were previously characterized by Fourier transform infra-red (FTIR) spectroscopy and found to be Type IaAB with N contents ranging from 13 ppm to 955 ppm (Stachel et al., 2018). Re-Os dating of peridotitic sulphide inclusions in Victor diamonds yielded a robust model-3 isochron age of 718 ± 49 Ma (Aulbach et al., 2018) for Victor diamond formation. Based on nitrogen content and aggregation state data, an average mantle residence temperature of 1140 ± 19 °C was obtained for a mantle residence time of 540 Ma, derived from the formation age and the emplacement of the Victor kimberlite (177 ± 4 Ma, ID-TIMS U-Pb perovskite age; Januszczak et al., 2013) (Stachel et al., 2018).

In addition to the Victor samples, gem diamond samples of lower clarity originating from different diamondiferous xenoliths from the Finsch and Newlands kimberlites, South Africa, have been analyzed. Four diamonds come from Newlands eclogite xenoliths. Nitrogen aggregation and concentration data obtained on one Newlands diamond yields a temperature of ~1100 °C at a residence time of 1000 Ma (Laiginhas et al., 2010), consistent with the clinopyroxene - garnet temperature from diamondiferous Roberts Victor xenolith RV124 (1097 °C – Taylor et al., 1995). The formation age of the Newlands diamonds is unknown; whole rock Re-Os dating of diamond bearing eclogites from the Newlands kimberlite, however, indicates that the eclogitic diamonds are likely of Archean age (Menzies et al., 2003). Four diamonds analysed in this study originate from two different Finsch harzburgite xenoliths (F866 and JJG). Nitrogen aggregation and concentration data of one diamond from the F866 xenolith yields a temperature of ~ 1125 °C (at a mantle residence time of 1000 Ma, Laiginhas et al., 2010) that agrees with previous data from

Taylor and Milledge (1995). All Finsch peridotitic diamonds analysed to date show Archean formation ages (3300-3200 Ma, Richardson et al., 1984).

2.1 Geology of diamond sample sources

2.1.1 Victor, Canada

De Beers' Victor Mine - the first diamond mine on the Superior Craton - is part of the Jurassic Attawapiskat kimberlite field, Ontario, Canada (Kong et al., 1999). It is a low-grade mine at 0.23 carats per tonne, but its diamond value is among the highest in the world (about US$440/ct).

The Victor Mine exploits a diamond resource that is principally (~85%) derived from lherzolitic mantle substrates (Aulbach et al., 2018; Stachel et al., 2018). Based on garnet inclusion trace element characteristics and geothermobarometric results, Victor diamonds formed under sub-solidus (lherzolite + H_2O) conditions in a narrow (<10 km thick) layer at about 180 km depth (Stachel et al., 2018). The young diamond age and lherzolitic association make Victor unique among known diamond mines worldwide.

2.1.2 Newlands, South Africa

The Newlands kimberlite cluster, located approximately 60 km NW of Kimberley, South Africa, is Cretaceous in age (114 ± 1.6 Ma) and classifies as a Group II kimberlite (Smith, 1983; Smith et al., 1985). Newlands consists of a series of five small pipes or "blows" located along a dyke. The mine, owned and operated since 2005 by Dwyka Diamonds Limited, has produced a wide variety of mantle xenoliths, including diamond-bearing harzburgites and eclogites (Gurney and Menzies, 1998).

2.1.3 Finsch, South Africa

The Finsch kimberlite pipe is located approximately 150 km west of Kimberley, South Africa, and was discovered in 1960 (Field et al., 2008)—diamond production commenced in 1965 (Viljoen and Lawless, 1988). Finsch is a Group II kimberlite pipe with a Rb–Sr emplacement age of 118 ± 2.8 Ma (Smith et al., 1985). Inclusions in Finsch diamonds are predominantly peridotitic (harzburgitic; Harris and Gurney, 1979; Tsai et al., 1979) with a Sm–Nd model age of 3300 ± 100 Ma (Richardson et al., 1984). Eclogitic inclusions were found to be significantly younger (1580 ± 50 Ma, Richardson et al., 1990; Sm–Nd model ages from 1443 ± 166 to 1657 ± 77 Ma, Smith et al., 1991).

3. Analytical methods

All laboratory and analytical work on the Victor diamond suite was carried out in the Arctic Resources Laboratory at the Department of Earth and Atmospheric Sciences, University of Alberta. The laboratory and analytical work on the Newlands and Finsch diamond suites was performed in the Arthur Holmes Isotope Geology Laboratory at the Department of Earth Science, University of Durham, using the same analytical procedures later adopted at the University of Alberta (summarized in McNeill et al., 2009).

3.1 Offline laser ablation

Diamond ablations were performed using an off-line laser ablation sampling technique developed by McNeill et al. (2009) and Klein-BenDavid et al. (2010) that utilizes a closed-system laser ablation cell in which a diamond is ablated and the products trapped, allowing the accumulation of much higher volumes of analyte compared to on-line methods. The custom-designed, sealed PFA ablation cell is capped with a pre-cleaned fused silica laser window that is blank tested in every analysis batch. Comparison of the method to on-line laser methods has been

documented by Klein-BenDavid et al. (2014). The closed nature of the cell and laser decomposition of the sample mean that detection limits can be improved simply by increasing the ablation time, providing increased analyte signal at constant "blank". The solution-based nature of the trace element analyses allows for calibration against matrix-matched standards. All these factors facilitate the production of quantitative data for the very low abundances of elemental impurities in gem diamonds.

3.1.1 Sample preparation

All diamonds were leached in 16N Seastar triple distilled UPA-grade HNO_3 and 29N UPA-grade HF on a hotplate at 100 °C for 24 hrs and then rinsed in 18.2 MΩ MQ H_2O before being leached in Teflon distilled 6N HCl for another 24 hrs at 100 °C, followed by a final rinse in MQ H_2O. All samples were dried and weighed on a Mettler Toledo™ UMT2 Micro Balance prior to placing them in the ablation cell. The diamond is held under its own weight, presenting a flat surface orthogonal to the laser beam. Once the diamond is in place the ablation cell is capped with the laser window.

3.1.2 Ablation and sample collection

Ablations of the Victor diamond suite were performed using a RESOlution M-50HR (Resonetics) 193 nm ArF Excimer (CompexPro 102, Coherent) laser ablation system. The system is equipped with a custom-designed cell holder mounted onto a high-precision stage (step resolution 0.02 µm), allowing the placement of up to 9 closed ablation cells. All ablations were performed using a raster pattern with the following ablation conditions: Energy density (fluence) 4–7 J/cm^2; repetition rate 100 Hz; spot size 90 µm. Ablation times varied from 3–8 h. The

analysed area of each diamond was optically free of solid inclusions or other impurities visible at the 10 micrometer scale.

Following ablation, the window was removed, 3 ml of 6N HCl UpA was added to the ablation cell and an acid-cleaned PFA Teflon cap was inserted to cover the cell. The sealed cell was then placed in an ultrasonic bath for 40 min. Subsequently the liquid was transferred from the ablation cell to a 7 ml Teflon beaker and dried on a hotplate at 100 °C. The dried ablation product was taken up in 1 ml 3 % HNO_3 for 48 hrs at 120 °C, with 500 ppt Ir and In added as internal standards, for trace element analysis.

Between two to four total procedural blanks (TPBs) were determined for each batch of samples processed, using the same ablation cells and reagents as used for the samples, to determine the average size of the blank contribution. The only step omitted was the step of ablating a solid. Including an ablation step would require a solid that is essentially devoid of all trace elements or have trace element concentrations below the LOD of our method (McNeill, 2011).

Diamonds were rinsed in MQ H_2O and dried before being re-weighed. The weight loss (0.01–0.98 mg) resulting from the ablation was then calculated. Detailed descriptions of the sample ablation and collection procedures for the Victor diamonds are given in McNeill et al. (2009) and Klein-BenDavid et al. (2010), for the Newlands and Finsch diamond analyses in McNeill et al. (2009).

3.2 Trace element analysis

The dilute HNO_3 solutions resulting from the ablation of the Victor diamonds, and their associated TPB solutions were analyzed for trace element concentrations on a Thermo Scientific Element XR2 magnetic sector ICPMS equipped with a JET interface, running at an RF power of

1320 W. Plasma cooling gas, auxiliary gas and nebulizer gas flow rates were 16 l min^{-1}, 0.82 l min^{-1} and 1.067 l min^{-1}, respectively. To increase plasma robustness and ICP sensitivity, N_2 was added into the central channel of plasma. An APEX-Q high-efficiency sample introduction system (Elemental Scientific Inc.) fitted with a membrane desolvation module (ACM - **A**ctively **C**ooled **M**embrane), was used for sample introduction.

At the start of each analytical session the mass spectrometer was tuned to optimize sensitivity for ^{7}Li, ^{115}In and ^{238}U using an Element standard tune solution. The oxide production rate was checked using 1 ppb solutions of Ce and U. Sensitivity is optimized to give low oxide generation whilst maintaining high overall sensitivity and CeO/Ce UO/U is maintained at <0.4 and 0.6 %, respectively.

In total 32 elements were analysed in either low (LR) or medium mass resolution (MR: $M/\Delta M \sim 4500$). The isotopes measured were: ^{52}Cr (MR), ^{55}Mn (MR), ^{56}Fe (MR), ^{59}Co (MR), ^{60}Ni (MR), ^{63}Cu (MR), ^{64}Zn (MR), ^{69}Ga (LR), ^{85}Rb (LR), ^{88}Sr (LR), ^{89}Y (LR), ^{90}Zr (MR), ^{93}Nb (LR), ^{98}Mo (LR), ^{133}Cs (LR), ^{137}Ba (LR), ^{139}La (LR), ^{140}Ce (LR), ^{141}Pr (LR), ^{143}Nd (LR), ^{147}Sm (LR), ^{151}Eu (LR), ^{157}Gd (LR), ^{161}Dy (LR), ^{165}Ho (LR), ^{167}Er (LR), ^{173}Yb (LR), ^{175}Lu (LR), ^{178}Hf (LR), ^{208}Pb (LR), ^{232}Th (LR) and ^{238}U (LR). Each analysis ran for 90-105 s with a 200 s wash (3 % UpA HNO_3) run in between every sample. Solution concentrations were measured against a 5-point calibration line derived from dilutions of a synthetic rock multi-element standard solution, MES-0314-01. The standard was diluted 50,000, 100,000, 250,000 and 500,000 times yielding concentrations in the range of 1 ppt to 35 ppb for different elements and different dilutions, thus providing an appropriate matrix-match for the samples so calibration lines did not require extrapolation into the region of sample analyte concentrations. All data were corrected for instrument drift and all sample concentrations were normalized to the weight loss of the diamond.

Weighted regression calibrations lines were used and the stated uncertainties on concentrations include fully propagated errors for the calibration line and sample weighing.

3.3 Limits of Quantification (LOQ)

Due to the extremely low concentrations of impurities in gem-quality diamonds it is important to have a robust knowledge of analytical blanks, to allow accurate estimates of the limits of quantification. In this study we use the limit of quantification (LOQ) as originally defined by Currie (1968): LOQ = 7σ (with σ = the standard deviation of the TPB). Further details are given in McNeill et al. (2009) and Klein-BenDavid et al. (2010).

A total of 13 total procedural blanks (TPBs) for the Victor diamond ablations were performed. Average TBPs were calculated using all acquired data, including values below the instrument detection limit (< IDL). Data with values of 0 and outliers whose values are either greater than UQ + 1.5 * IQR or less than LQ - 1.5 * IQR (with UQ = upper quartile, LQ = lower quartile, IQR = Inter-quartile range) were winsorized (Tukey, 1962) to minimize the influence of outliers. The values of high outlier data points were converted to the value of the highest data point not considered an outlier; all points with a value of 0 were converted to the LOD. As the distribution of data can be heavily influenced by outliers, setting all outliers to a specified percentile of the data, results in estimators that are more robust to outliers. The repeatability of blanks yielded consistently low values so that our LOQs for the elements Y, Nb, Cs, La, Pr, Nd, Sm, Eu, Gd, Tb, Dy, Ho, Er, Yb, Lu, Th, and U are less than 1 pg, for the elements Co, Rb, Ce and Hf less than 5 pg, for the elements Mn, Sr, Zr, Mo and Ba less than 40 pg, and for the elements Cr, Fe, Ni, Cu and Zn less than 1.2 ng.

We use LOQ as an important data quality filter, as opposed to the limit of detection – defined as ‘the true net signal level that may be expected a priori to lead to detection’ (Currie, 1968). Limit

of detection is often used as a data cut off filter by authors using direct laser ablation approaches to diamond analysis (e.g., Rege et al., 2005, Tomlinson et al., 2005, Zedgenizov et al., 2007). The LOD cut off only provides confidence that a signal has been detected, yet the best-case uncertainty on concentrations at or just above LOD are ± 92 % at the 95 % confidence level compared to ± 40 % for LOQ using the 7 σ cut off (Taylor, 1987). As such, in presenting the data we have calculated three different median values for all analysed elements for the Victor diamonds, on for all acquired data, one for all acquired data, one for all acquired data > LOD (3 σ) and one for all data > LOQ (7 σ). As can be seen in the chondrite normalized multi-element pattern in Fig. 1, the pattern does not change significantly. However, the concentrations of the very low abundance elements change to significantly higher values when only values > LOQ are included. Because of the exceptionally low concentrations of some trace elements in Victor diamonds we discuss and show some data that are > LOD but < LOQ but in doing so, we emphasise that such data is merely "indicative" and not fully quantitative. The reported median values, 25 % quartiles and 75 % quartiles for the Victor data encompass all acquired data, including data ≤ LOD. In order to account for differences in concentration that are the result of differences in the inclusion content in the diamonds all data is normalized to $Er_N = 1$ before calculation of the median.

The accuracy of the off-line ablation method has been verified by Klein-BenDavid et al. (2014) by comparison to data produced by a high concentration fibrous diamond. The reader is referred to that publication for details of accuracy.

4. Results

4.1 Victor

Trace element concentrations of the Victor diamond suite are very low, with all samples being highly depleted relative to chondrite abundances (Table S1, Fig. 2A, 3A). Elemental abundances of rare earth elements (REE) along with Nb, Th, and U range from 10s of ppt to 10s of ppb and large ion lithophile elements (LILE) such as Cs, Rb and Ba range from 100s of ppt to 100s of ppb. Transition metals such as Cr, Mn and Fe range from ppb levels up to 100s of ppm (Fig. A1). Absolute trace element abundances in gem diamonds, as in fibrous diamonds, are, however, primarily a function of the inclusion density. Double-normalized (Chondrite-normalized (N) multiplied with $1/Er_N$) trace element patterns show a wide range in relative enrichment of light rare earth elements (LREE) compared to heavy rare earth elements (HREE), with La_N/Yb_N of 2–57 (Fig. 3A). Differences are evident between the REE_N patterns of diamonds containing silicate (median $La_N/Yb_N \sim 17$) and sulphide inclusions (median $La_N/Yb_N \sim 10$).

In general, the sulphide-bearing diamonds have lower REE contents than the silicate-bearing diamonds, but the ranges overlap. When multi-element patterns are considered, the sulphide-bearing diamonds show a smaller degree of inter-element fractionation than the silicate-bearing diamonds (Fig. 2A). This observation can be quantified through elemental ratios using the most robust data. For instance, Ba_N/Nb_N (silicate-included median 0.18; sulphide-included median 1.2) and Sm_N/Hf_N (silicate-included median 0.05; sulphide-included median 0.8) are significantly more fractionated in the silicate-bearing diamonds at Victor (Fig. 4). A statistical comparison using the equal variance t-test (Fisher, 1925), indicates that there is a greater than 95% probability that the sulphide-bearing and silicate-bearing diamonds are drawn from different populations based on their La_N/Yb_N, Ba_N/Nb_N and Sm_N/Hf_N values. However, it is important to note that due to the small number of samples (n = 8 for each population) this result is only qualitative; non-normal distributions are only quantifiable for larger sample sizes (Ruxton, 2006).

As a suite, the Victor silicate-bearing diamonds are characterized by positive Cs, Ce, Y and Zr-Hf anomalies. Lutetium is high relative to the other HREE. The Victor sulphide-bearing diamonds show a slight positive Ce anomaly and positive Zr-Hf anomalies. Two of the sulphide bearing diamonds, V2-01 and V2-07, show highly fractionated multi-element patterns that are characterised by positive Ce and Cs anomalies (Fig. A2). Both diamonds have a distinct appearance to other sulphide-bearing Victor diamonds through a high density of small sulphide inclusions throughout the crystals. Consequently, for these two diamonds, minute (< 1 μm) sulphide inclusions were probably included in the analyte.

Concentrations of transition metals such as Ni, Fe and Co vary more widely for the diamonds containing sulphide inclusions than for the silicate-included diamonds (Fig. A1) and concentrations of Cu, Fe, Ni, Zn and Co are higher for the former, especially in V2-01, V2-07 and V2-09, perhaps again reflecting the ablation of sub-micron invisible sulphides.

4.2 Newlands and Finsch

Trace element concentrations in both Newlands and Finsch diamonds are much higher (in some cases up to three orders of magnitude) than those of Victor diamonds, correlating broadly with their lower clarity. Elemental abundances of REE along with Nb, Th, and U range from 100s of ppt to 100s of ppm for the Newlands diamonds and from 100s of ppt to 10s of ppm for the Finsch diamonds, overlapping the range of concentrations in fibrous diamonds. LILE such as Rb, Sr and Ba range from lower ppb levels to 100s of ppm for both Newlands and Finsch. Two Finsch diamonds have Ba concentrations in excess of 1000 ppm (Table S1). Double-normalized (Chondrite-normalized (N) multiplied with $1/Er_N$) REE patterns for Newlands and Finsch diamonds show strong enrichment of LREE compared to HREE, with La_N/Yb_N of 12–230 (median 68) for Newlands and 9–561 (median 34) for Finsch diamonds (Fig. 3B, 4).

Both suites show higher and more variable inter-element fractionation than the Victor diamonds with Ba_N/Nb_N of 0.4–38 for Newlands and 3–3007 for Finsch and Sm_N/Hf_N of 0.2–5 for Newlands and 0.04–12 for Finsch. The Newlands diamonds are characterized by negative Nb and Zr-Hf anomalies (Fig. 2B). As a suite, the Finsch diamonds display positive Sr, Ba and Y anomalies (Fig. 2B). By far the highest Ba anomalies are observed in the two Finsch diamonds from harzburgite xenolith F866 (Fig. A3). Two Finsch diamonds (JJG1 and F8662) also show positive Zr-Hf anomalies, one sample (JJG4) shows a negative Zr-Hf anomaly and one a positive Eu anomaly (JJG1). The two Finsch diamonds originating from the more depleted harzburgitic xenoliths (JJG) are, in addition, characterized by a negative Nb anomaly. Overall, the eclogitic Newlands and peridotitic Finsch diamonds show very similar trace element characteristics, but differ in Ba, Sr and Zr-Hf, with the Newlands diamonds displaying no or negative anomalies in Ba and Sr and negative Zr-Hf anomalies whereas the Finsch diamonds have positive Ba, Sr and, with one exception, Zr-Hf anomalies.

5. Discussion

5.1 Origin of the trace element signatures

While it has long been established that fibrous diamonds grow from carbon-bearing fluids (typically termed HDFs in the literature) that can be found (as an end-product of the diamond forming reactions) as micro- to nano-inclusions in most fibrous diamonds (e.g., Klein-BenDavid et al., 2004; Shiryaev et al., 2005), the mechanism of formation for gem diamond has remained ambiguous. A genetic relationship between fibrous and gem diamonds has recently been affirmed through the finding that HDFs of similar major element composition occur in fibrous and in gem diamonds (Jablon and Navon, 2016).

Further indications for a similarity of fluids/melts in fibrous and gem diamonds can be derived from rare analyses of trace elements in gem diamonds that are above limits of quantification. For instance, in a gem diamond from Akwatia, Ghana, Melton et al. (2012) found a trace element pattern very similar in shape to low-Mg carbonatitic HDFs in fibrous diamonds, but at far more dilute concentrations. The trace element patterns of the other gem diamonds analysed by Melton et al. (2012), however, did not yield a faithful representation of the diamond source fluids, but were interpreted to reflect complex and variable mixtures of minute mineral inclusions instead.

The double-normalized REE patterns of the Victor, Finsch and Newlands diamonds are quite smooth and linear, and characterized by shallow negative LREE-HREE slopes (Fig. 5), similar to those commonly found in fibrous diamonds, albeit at much lower concentrations (e.g., Zedgenizov et al., 2009; Weiss et al., 2009, 2011; Tomlinson et al., 2009; McNeill et al., 2009; Klein-BenDavid et al., 2010). This similarity clearly indicates that fluid/melt inclusions ≤25 nm (Melton et al., 2012) dominate the chemical signature of gem diamonds with trace element systematics similar to those observed in fibrous diamonds.

5.2 Trace elements in high-purity gem diamonds from Victor

Differences in the trace element patterns of Victor diamonds broadly align with the division into sulphide- and silicate-included samples. Silicate inclusion-bearing diamonds have generally more fractionated REE patterns and show greater inter-element fractionations for element ratios such as Ba_N/Nb_N and Sm_N/Hf_N. The distinct positive slope in the HREE, from Er to Lu for the silicate-bearing and from Yb to Lu for the sulphide-bearing diamonds (Fig. 5B), is similar to REE patterns of subcalcic garnets and likely represents a remnant signature of the primary melt-depletion affecting all peridotitic diamond substrates (Stachel et al., 1998). The most significant differences between the two Victor groupings are positive Cs, Ce and Y anomalies and a negative

Sr anomaly present in silicate-bearing but not in sulphide-bearing diamonds. Stachel et al. (2018) showed that Victor diamonds formed under sub-solidus conditions (lherzolite + H_2O) at the depth where upward percolating melts freeze. Such freezing melts could have been the source of the diamond-forming HDFs at Victor. The shallow slope of the chondrite-normalized diamond trace element patterns is, however, inconsistent with highly fractionated diamond forming fluids that derive from low volume melts formed during incipient melting (1-2% melting; Green and Folloon, 1998), but resembles melts formed during major melting instead. A La_N/Yb_N of ~ 17 in Victor diamond-forming HDFs corresponds to 10% melt extraction from a primitive mantle source, which at sublithospheric pressures (> 6 GPa) would yield a silicate melt intermediate between primitive kimberlite (La_N/Yb_N ~ 110, Becker and Le Roex, 2006) and komatiite (La_N/Yb_N ~ 0.4 – 1.6, Wilson et al., 2003).

As Weiss et al. (2013) have shown, diamond forming fluids swiftly fractionate during percolation through the lithosphere, suggesting that HDFs with flat, unfractionated trace element patterns may only have experienced limited interaction with lithospheric wall rocks. At Victor, both the sulphide inclusion-bearing and the silicate inclusion-bearing diamond suites have relatively flat trace element patterns, but from the more fractionated pattern for silicate inclusion-bearing diamonds it may be inferred that sulphide-included diamonds crystallized somewhat deeper, closer to the HDF source. Increased interaction with wall-rock peridotite for the HDFs associated with silicate inclusions may have included precipitation of or equilibration with (1) clinopyroxene, causing negative Sr anomalies, and (2) potential dissolution of mica (±ilmenite or rutile) leading to variable relative increases in Cs, Nb, La, Zr and Hf. Positive Ce anomalies in the more fractionated HDFs for silicate included diamonds may indicate interaction with a subducted crustal (biosiliceous and/or volcaniclastic) component (Bellot et al., 2018). Other processes and conditions able to generate Ce anomalies - oxygen fugacity, the presence of

residual mineral phases, partial melting, or the involvement of aqueous fluids resulting from the dehydration of recycled material - cannot be definitely ruled out in producing Ce anomalies, however, the proportion of Ce^{4+} for these redox conditions was shown to be extremely low. Rege et al. (2010) related the occurrence of negative Y anomalies in their diamond trace element patterns to the fractionation of fluorite from the diamond forming medium. If such anomalies are not simply related to analytical scatter at low concentrations of the neighbouring elements Dy and Ho (Fig. 2A), a positive Y anomaly in the silicate-associated HDFs may reflect the reverse process, dissolution of fluorite, or more likely fluorapatite (both have positive Y anomalies; Bühn et al., 2001, 2002), precipitated during or preceding kimberlite or carbonatite metasomatism. As an alternative to different degrees of fractionation and assimilation *en route* to diamond formation, the HDFs forming the sulphide- and silicate-bearing diamonds could also relate to subtly different primary sources.

5.3 Comparison with other gem diamonds

The results for the high-quality gem diamonds from Victor agree with the findings of McNeill et al. (2009) who analysed gem quality diamonds from the Cullinan Mine (previously known as Premier), South Africa. The Cullinan diamonds contain predominantly eclogitic silicate inclusions. Similar to our results for Victor, McNeill et al. (2009) reported relatively unfractionated trace element patterns, with no significant elemental anomalies, very low levels of REE_N and modest levels of enrichment of $LREE_N$ over $HREE_N$. There are, however, some differences between Cullinan and Victor HDFs, namely negative Sr, Ce, Y and Zr anomalies (Fig. 6) a positive Eu anomaly and, in some instances, more pronounced enrichment in LILE over Nb in the Cullinan diamonds (Fig. A4). In addition, the REE patterns are slightly more fractionated than for the Victor diamonds. These overall subtle differences between Victor and

Cullinan diamond-forming HDFs may relate to differences in the nature and extent of wall-rock interaction prior to or during diamond formation.

5.4 Comparison with fibrous, fluid-rich diamonds

To compare the Victor, Newlands and Finsch HDFs to typical trace element patterns for fluid-rich diamonds, we normalized the latter to Er_N=1. This eliminates the large variations in trace element concentrations that are due to different fluid inclusion concentrations, in particular when comparing fibrous and gem diamonds (Fig. 7).

This double normalization emphasises that Victor diamond fluids, with their shallow negative LREE-HREE slopes, most closely resemble the planed trace element pattern of Weiss et al. (2013). The Cullinan diamond suite also has a shallow negative LREE-HREE slope but more closely resembles the ribbed end-member of HDFs in fibrous diamonds (Weiss et al., 2013), although with a shallower slope. The Newlands diamond suite also most closely resembles the 'ribbed' pattern. The patterns for the Finsch diamond suite fall in between both end-members (Fig. 7).

The trace element systematics of gem diamonds appear to be broadly similar to those of fluid-rich diamonds from a variety of locations and, thus also correspond to similar end-member types of HDFs. The trace element characteristics of the Victor diamond suite corresponds most closely to fibrous diamonds with Mg-carbonatitic HDF inclusions studied by Klein-BenDavid et al. (2014) and to the less fractionated patterns of silicic to low-Mg carbonatitic fluids (Fig. 8). The silicate-bearing Victor diamonds also display the negative Sr anomaly observed in high Mg-carbonatitic fluids.

The Newlands gem diamonds have La_N/Nb_N and Ba_N/Nb_N in the range of both high Mg-carbonatitic and silicic to low-Mg carbonatitic fluids reported by Klein-BenDavid et al. (2014). The Th_N/Nb_N ratios are, however, much higher at Newlands, indicating that these diamonds likely formed from a silicic to low-Mg carbonatitic fluid, with the elevated Th perhaps indicating a higher H_2O component in the fluid as Th is an element thought to be mobile in hydrous fluids in the mantle (e.g., Elliot et al., 1997). Silicic to low Mg-carbonatitic HDFs for the eclogitic Newlands diamonds suite are consistent with the observation of Weiss et al. (2015) that silicic HDFs occur exclusively together with eclogitic mineral inclusions of omphacitic clinopyroxene.

The very similar trace element characteristics of the Cullinan diamonds indicate likely formation from a silicic to low-Mg carbonatitic fluid as well, also consistent with their predominantly eclogitic paragenesis (Fig. 8).

The trace element characteristics of the Finsch diamond suite is most similar to saline HDFs (Smith et al., 2012; Weiss et al., 2013, 2015) (Fig. 9 and A5) – the key feature is the very high Ba content, resulting in elevated Ba_N/Nb_N ratios (Fig. 8). In addition, the patterns display prominent positive Sr anomalies and the REE_N pattern of one diamond (JJG1) shows a positive Eu anomaly.

The strong similarity between the trace element systematics of Finsch gem diamonds and saline fluids in cloudy and fibrous diamonds from Finsch, Wawa, Ekati and Diavik (Fig. A5) strongly supports a close link between the parental fluids of gem and fluid-rich fibrous diamonds, showing that highly saline diamond-forming fluids extend beyond fibrous diamonds. The high Ba/Nb, positive Sr and positive Eu anomalies of saline HDFs have been linked to a subduction origin (Weiss et al., 2015). In a recent study Weiss and Goldstein (2018) identified two microinclusion-bearing diamond populations from Finsch: 'Finsch IaA' diamonds with nitrogen aggregation solely in A-centers containing saline HDF microinclusions, and 'Finsch IaAB' diamonds with nitrogen in both A- and B-centers, that contain microinclusions with carbonatite

HDF compositions. Based on nitrogen aggregation states and estimates for mantle residence temperatures, they suggest the formation of 'Finsch IaA' and 'Finsch IaAB' diamonds during two separate metasomatic events, a young saline metasomatic event that preceded kimberlite eruption for the 'Finsch IaA' diamonds, and an older event for formation of 'Finsch IaAB'. Combined data for microinclusion-bearing diamonds from the Finsch Group II kimberlite and the neighbouring Group I kimberlites at Koffiefontein and De Beers Pool leads the authors to assert that a substantial volume of the southwest Kaapvaal deep lithosphere was impacted by saline metasomatism during Cretaceous time. At least one of the gem diamonds from Finsch harzburgites reported here is Type IaAB (Laiginhas et al., 2010), similar to the 'FinschIaAB' diamonds of Weiss and Goldstein (2018). While it is possible that there is a late-stage overgrowth on some of the saline fluid-bearing gem diamonds analysed here, luminescence imaging and FTIR data of diamond F866 1 show no evidence of such an overgrowth. Instead it appears homogenous in its internal texture. The saline HDFs in Finsch gem diamonds are indicative of an older saline metasomatic event at Finsch, in addition to the younger infiltration of saline fluids into the lithospheric mantle demonstrated by Weiss and Goldstein (2018). The Finsch Group II kimberlite is characterised by strong whole-rock Ba enrichment and very low ε_{Nd} (Fraser et al., 1985). The unradiogenic Nd isotope characteristics of the Finsch kimberlite may have resulted from ancient LREE enrichment of the lithospheric mantle source region before diamond formation billions of years ago (Richardson et al., 1984). Similarly, the elemental characteristics of the Finsch harzburgitic diamonds, specifically their saline nature, may also reflect this ancient, potentially subduction-related enrichment event.

In summary, the trace element characteristics of diamond-forming fluids in the eclogitic Cullinan and Newlands diamond suites indicate diamond formation from a silicic to low-Mg carbonatitic fluid, consistent with the equilibration of originally asthenospheric fluids with

eclogitic wall rocks during a fractional percolation process (Weiss et al., 2009, 2015). The trace element characteristics of the Victor diamonds are most consistent with high Mg-carbonatitic HDFs in fibrous diamonds. Such high-Mg carbonatitic HDFs are thought to originate from a carbonated peridotite source, either within the lithosphere or in the asthenosphere (Weiss et al., 2009, 2011; Klein-BenDavid et al., 2014). The Finsch diamonds trapped saline HDFs, suggesting fluid derivation from recycled oceanic crust, but considerably earlier than the saline fluid metasomatism documented by 'Finsch IaA' diamonds.

6. Summary and Conclusions

The concentrations of a wide range of elements have been determined in a suite of inclusion-bearing diamonds from the Victor kimberlite, Ontario, Canada. The concentrations of most trace elements, including Ba, Nb, U, Y and REEs, for gem diamonds from the Victor diamond mine are very low, significantly lower than values reported for fibrous stones but consistent with "closed-cell" ablation data previously reported for gem diamonds from other mines (e.g., McNeill et al., 2009). Trace element concentrations for less pure but monocrystalline, fluid-poor diamonds from Newlands and Finsch are up to three orders of magnitude higher, correlating broadly with their lower clarity.

Differences are evident in the REE_N patterns of Victor diamonds containing silicate inclusions (median $La_N/Yb_N \sim 17$) and sulphide inclusions (median $La_N/Yb_N \sim 10$). In addition to less fractionated REE patterns, the sulphide-bearing diamonds also have more widely varying Ni, Fe and Co concentrations. Although significant, these differences are relatively subtle and not consistent across all key trace element ratios; therefore, it seems likely that the fluids precipitating Victor diamonds have broadly the same origin, but that silicate- and sulphide-

bearing diamonds either formed at different stages of the same evolutionary processes or from fluids with subtly different sources.

Our high quality trace element data for gem diamonds show many similarities to those reported for fluid-rich fibrous diamonds. We establish that "planed" and "ribbed" trace element patterns characterise not only the HDF inclusions in fibrous diamonds but also in gem diamonds. For diamonds from two Finsch harzburgite xenoliths, based on similarities in trace element patterns, we also present the first evidence for the involvement of saline fluids in the precipitation of gem diamonds. Since saline HDFs are thought to originate from subducted oceanic crust (Weiss et al., 2015), this establishes a link between formation of diamond in harzburgitic substrates and subduction, possibly dating back as far as ~3300-3200 Ma (Richardson et al., 1984). The studied gem diamonds come from mines where Paleoarchean to Neoproterozoic formation ages were determined and contain the same spectrum of HDFs recorded in fibrous diamonds, documenting formation of both types of diamonds from HDFs spanning similar ranges in composition over billions of years (c.f. Smith et al., 2012).

The formation of Victor diamonds largely occurred under sub-solidus (lherzolite + H_2O) conditions (Stachel et al., 2018). Yet, the shallow negative LREE-HREE slopes displayed by Victor (and Cullinan) diamonds establish a signature indicative of original derivation of the diamond forming agent during major melting (~10 % melt). Consequently, this signature must have been passed on to HDFs separating from such silicate melts. Experimental work (e.g., Bureau et al., 2012) showed that hydrous silicate melt and aqueous fluid can coexist in regions of active diamond growth. Limited available experimental data suggest that fractionation of REE between hydrous-silicic fluids and silicate melt (basanite) at high pressure and temperature is

minor (Adam et al., 2014). Nevertheless, the fairly primitive trace element patterns of planed diamond-forming HDFs remain enigmatic.

Acknowledgements

We thank De Beers Canada for supplying the Victor samples. This research was funded by a CERC award to Graham Pearson. Thank you to the reviewers, Oded Navon and Sami Mikhail and the editor, Andrew Kerr, for providing constructive comments that improved this paper.

Supplementary data

Supplementary material

References

Adam, J., Locmelis, M., Afonso, J.C., Rushmer, T., Fiorentini, M.L., 2014. The capacity of hydrous fluids to transport and fractionate incompatible elements and metals within the Earth's mantle. Geochemistry, Geophysics, Geosystems 15(6), 2241-2253.

Aulbach, A., Creaser. R.A., Stachel, T., Heaman, L.M., Chinn, I., Kong, J., 2018. Sulphide inclusions in diamond from Victor (Superior craton): Intra-mantle cycling of Os and volatiles (C,N,S) during plate reorganisation. Earth and Planetary Science Letters 490, 77-87.

Becker, M., Le Roex, A.P., 2006. Geochemistry of South African on- and off-craton Group I and II kimberlites: petrogenesis and source region evaluation. Journal of Petrology 47, 673-703.

Bellot, N., Boyet, M., Doucelance, R., Bonnand, P., Savov, I.P., Plank, T., Elliott, T., 2018. Origin of negative cerium anomalies in subduction-related volcanic samples: Constraints from Ce and Nd isotopes. Chemical Geology 500, 46-63.

Bühn, B., Wall, F., Le Bas, M.J., 2001. Rare-earth element systematics of carbonatitic fluorapatites, and their significance for carbonatitic magma evolution. Contributions to Mineralogy and Petrology 141, 572-591.

Bühn, B., Rankin, A.H., Schneider, J., Dulski, P., 2002. The nature of orthomagmatic, carbonatitic fluids precipitating REE, Sr-rich fluorite: fluid-inclusion evidence from the Okorusu fluorite deposit, Namibia. Chemical Geology 186, 75-98.

Bureau, H., Langenhorst, F., Auzende, A.-L., Frost, D.J., Estève, I., Siebert, J., 2012. The growth of fibrous, cloudy and polycrystalline diamonds. Geochimica et Cosmochimica Acta 77, 202-214.

Burgess, R., Turner, G., Laurenzi, M., Harris, J. W., 1989. 40Ar/39Ar laser probe dating of individual clinopyroxene inclusions in Premier eclogitic diamonds. Earth and Planetary Science Letters 94, 22-28.

Currie, L.A., 1968. Limits for qualitative detection and quantitative determination. Analytical Chemistry 40, 586.

Elliot, T., Plank, T., Zindler, A., White, W. Bourdon, B., 1997. Element transport from slab to volcanic front at the Mariana arc. Journal of Geophysical Research 102, 14,991-15,019.

Field, M., Stiefenhofer, J., Robey, J., Kurszlaukis, S., 2008. Kimberlite-hosted diamond deposits of southern Africa: A review. Ore Geology Reviews 34, 33-75.

Fisher, R.A., 1925. Statistical Methods for Research Workers. Oliver and Boyd (Edinburgh).

Fraser, K.J., Hawkesworth, C.J, Erlank, A.J., Mitchell, R.H., Scott-Smith, B.H., 1985. Sr, Nd and Pb isotope and minor element geochemistry of lamproites and kimberlites. Earth and Planetary Science Letters 76, 57-70.

Green, D.H., Falloon, T.J., 1998. Pyrolite: a Ringwood concept and its current expression, in: Jackson, I. (ed.), The Earth's mantle, Cambridge University Press, Cambridge, pp. 311-378.

Gurney, J.J., Menzies, A.H., 1998. The Newlands kimberlite pipes and dyke complex. Small Mines Field Excursion guide. 7th International Kimberlite Conference. Cape Town, South Africa, 23-30.

Gurney, J.J., Helmstaedt, H.H., Richardson, S.H., Shirey, S.B., 2010. Diamonds through time. Economic Geology 105, 689-712.

Harris, J.W., Gurney, J.J., 1979. Inclusions in diamond, in: Field, J.E., (ed.), The properties of diamond. Academic Press, London, pp. 555-591.

Izraeli, E.S., Harris, J.W., Navon, O., 2001. Brine inclusions in diamonds: a new upper mantle fluid. Earth and Planetary Science Letters 187, 323-332.

Jablon, B.M., Navon, O., 2016. Most diamonds were created equal. Earth and Planetary Science Letters 443, 41-47.

Klein-BenDavid, O., Wirth, R., Navon, O., 2006. TEM imaging and analysis of microinclusions in diamonds: A close look at diamond-growing fluids. American Mineralogist 91, 353-365.

Klein-BenDavid, O., Izraeli, E.S., Hauri, E., Navon, O., 2007. Fluid inclusions in diamonds from the Diavik mine, Canada and the evolution of diamond-forming fluids. Geochimica et Cosmochimica Acta 71, 723-744.

Klein-BenDavid, O., Pearson, D.G., Nowell, G.M., Ottley, C., McNeill, J.C.R., Cartigny, P., 2010. Mixed fluid sources involved in diamond growth constrained by Sr–Nd–Pb–C–N isotopes and trace elements. Earth and Planetary Science Letters 289, 123-133.

Klein-BenDavid, O., Pearson, D.G., Nowell, G.M., Ottley, C., McNeill, J.C.R., Logvinova, A., Sobolev, N. V., 2014. The sources and time-integrated evolution of diamond-forming fluids – Trace elements and isotopic evidence. Geochimica et Cosmochimica Acta 125, 146-169.

Kong, J.M., Boucher, D.R., Scott Smith, B.H., 1999. Exploration and geology of the Attawapiskat kimberlites, James Bay Lowland, Northern Ontario, Canada. Proceedings of the 7th International Kimberlite Conference 1, Red Roof Design, Cape Town, South Africa, 452–467.

Laiginhas, F., Pearson, D.G., McNeill, J., Gurney, J.J., Nowell, G.M., Ottley, C.J., 2010. Origins of diamond-forming fluids: An isotopic and trace element study of diamonds and silicates from diamondiferous xenoliths. EGU General Assembly 2010, Vienna, Austria, EGU2010-3324.

McDonough, W. F., Sun, S.-S., 1995. The composition of the Earth. Chemical Geology 120, 223-253.

McNeill, J., Pearson, D.G., Klein-Bendavid, O., Nowell, G.M., Ottley, C.J., Chinn, I., 2009. Quantitative analysis of trace element concentrations in some gem-quality diamonds. Journal of Physics: Condensed Matter 21, 364207.

McNeill, J.C.R., 2011. New techniques for trace element and radiogenic isotope measurement of diamonds: their application to diamond petrogenesis and source tracing. Durham theses, Durham University. Available at Durham E-Theses Online: http://etheses.dur.ac.uk/713/

Melton, G.L., McNeill, J., Stachel, T., Pearson, D.G., Harris, J.W., 2012. Trace elements in gem diamond from Akwatia, Ghana and DeBeers Pool, South Africa. Chemical Geology 314-317, 1-8.

Menzies, A.H., Carlson, R.W., Shirey, S.B., Gurney, J.J., 2003. Re–Os systematics of diamond-bearing eclogites from the Newlands kimberlite. Lithos 71, 323-336.

Navon, O., Hutcheon, I., Rossman, G., Wasserburg, G., 1988. Mantle-derived fluids in diamond micro-inclusions. Nature 335, 784-789.

Pearson, D.G., Shirey, S.B., 1999. Isotopic dating of diamonds. SEG Reviews in Economic Geology 9, 143-171.

Pearson, D.G., Shirey, S.B., Bulanova, G.P., Carlson, R.W., Milledge, J., 1999. Dating and paragenetic distinction of diamonds using the Re-Os isotope system: Application to some Siberian diamonds, in: Gurney, J.J., Gurney, J.L., Pascoe, M.D., Richardson, S.H., (eds.), Proceedings of the 7th International Kimberlite Conference, Vol. 2, P.H. Nixon Volume: Cape Town, 637–643.

Phillips, D., Onstott, T. C., Harris, J. W. 1989. 40Ar/39Ar laser-probe dating of diamond inclusions from the Premier kimberlite. Nature 340, 460–462.

Rege, S., Jackson, S., Griffin, W.L., Davies, R.M., Pearson, N.J., O'Reilly, S.Y., 2005. Quantitative trace-element analysis of diamond by laser ablation inductively coupled plasma mass spectrometry: Journal of Analytical Atomic Spectrometry 20, 601-611.

Rege, S., Griffin, W.L., Pearson, N.J., Araujo, D., Zedgenizov, D., O'Reilly, S.Y., 2010. Trace-element patterns of fibrous and monocrystalline diamonds: Insights into mantle fluids. Lithos 118, 313-337.

Richardson, S.H., Gurney, J.J., Erlank, A.J., Harris, J.W., 1984. Origin of diamonds in old enriched mantle. Nature 310, 198-202.

Richardson, S.H., 1986. Latter-day origin of diamonds of eclogitic paragenesis. Nature 322, 623-626.

Richardson, S.H., Erlank, A.J., Harris, J.W., Hart, S.R., 1990. Eclogitic diamonds from of Proterozoic age from Cretaceous kimberlites. Nature 346, 54-56.

Richardson, S.H., Harris, J.W., Gurney,J.J., 1993. Three generations of diamonds from old continental mantle. Nature 366, 256-258.

Ruxton, G.D., 2006. The unequal variance t-test is an underused alternative to Student's t-test and the Mann–Whitney U test. Behavioral Ecology 17 (4), 688–690.

Shiryaev, A.A., Izraeli, E.S., Hauri, E.H., Zakharchenko, O.D., Navon, O., 2005. Chemical, optical and isotopic investigation of fibrous diamonds from Brazil. Russian Geology and Geophysics 46, 1185-1201.

Shirey, S.B., Richardson, S.H., 2011. Start of the Wilson Cycle at 3 Ga Shown by Diamonds from Subcontinental Mantle. Science 333, 434-436.

Smit, K. V., Shirey, S. B., Richardson, S. H., le Roex, A. P., Gurney, J. J., 2010. Re-Os isotopic composition of peridotitic sulphide inclusions in diamonds from Ellendale, Australia: Age

constraints on Kimberley cratonic lithosphere. Geochimica et Cosmochimica Acta 74, 3292-3306.

Smit, K. V., Shirey, S. B., Stern, R.A., Steele, A., Wang, W., 2016. Diamond growth from C–H–N–O recycled fluids in the lithosphere: Evidence from CH4 micro-inclusions and δ13C–δ15N–N content in Marange mixed-habit diamonds. Lithos 265, 68-81.

Smith, C.B., 1983. Pb, Sr, and Nd isotopic evidence for sources of African kimberlite. Nature 304, 51-54.

Smith, C.B., Gurney, J.J., Skinner, E.M.W., Clement, C.R., Ebrahim, N., 1985. Geochemical character of southern African kimberlites: a new approach based on isotopic constraints. Transactions of the Geological Society of South Africa 88, 267-280.

Smith, C.B., Gurney, J.J., Harris, J.W., Otter, M.L., Kirkley, M.B., Jagoutz, E., 1991. Neodymium and strontium isotope systematics of eclogite and websterite paragenesis inclusions from single diamonds, Finsch and Kimberley Pool, RSA. Geochimica et Cosmochimica Acta 55, 2579-2590.

Smith, E.M., Kopylova, M.G., Nowell, G.M., Pearson, D.G., Ryder, J., 2012. Archean mantle fluids preserved in fibrous diamonds from Wawa, Superior craton. Geology 40, 1071- 1046.

Stachel, T., Viljoen, K.S., Brey, G., Harris, J.W., 1998. Metasomatic processes in lherzolitic and harzburgitic domains of diamondiferous lithospheric mantle: REE in garnets from xenoliths and inclusions in diamonds. Earth and Planetary Science Letters 159, 1-12.

Stachel, T., Harris, J.W., 2008. The origin of cratonic diamonds − Constraints from mineral inclusions. Ore Geology Reviews 34, 5-32.

Stachel, T., Banas, A., Aulbach, S., Smit, K.V., Wescott, P., Chinn, I., Kong, J., 2018. The Victor Mine (Superior Craton, Canada): Neoproterozoic lherzolitic diamonds from a thermally-modified cratonic root. Mineralogy and Petrology, doi.org/10.1007/s00710-018-0574-y.

Sunagawa, I., 1984. Morphology of natural and synthetic diamond crystals, in: Sunagawa, I. (Ed.), Materials Science of the Earth's Interior. Terra Science, Tokyo, 303-330.

Taylor, J.K., 1987. Quality assurance of chemical measurements. Lweis Publishers, Chealsea, MI.

Taylor, W.R., Milledge, H.J., 1995. Nitrogen aggregation character, thermal history, and stable isotope composition of some xenolith-derived diamonds from Roberts Victor and Finsch. Extended abstracts of the 6th International Kimberlite Conference, Novosibirsk, Russia, 620-622.

Timmerman, S., Yeow, H., Honda, M., Howell, D., Jaques, A.L., Krebs, M., Woodland, S., Pearson, D.G., Avila, J.N., and Ireland, T.R. (2018): U-Th/He dating of fluid-rich 'fibrous' diamonds - a history of Phanerozoic diamond growth. *Submitted to Chemical Geology*.

Tomlinson, E., De Schrijver, I., De Corte, K., Jones, A.P., Moens, L., Vanhaecke, F., 2005. Trace element compositions of submicroscopic inclusions in coated diamond: A tool for understanding diamond petrogenesis. Geochimica et Cosmochimica Acta 69, 4719-4732.

Tomlinson, E.L., Jones, A.P., Harris, J.W., 2006. Co-existing fluid and silicate inclusions in mantle diamond: Earth and Planetary Science Letters 250, 581-595.

Tomlinson, E.L., Müller, W., Eimf, 2009. A snapshot of mantle metasomatism: Trace element analysis of coexisting fluid (LA-ICP-MS) and silicate (SIMS) inclusions in fibrous diamonds. Earth and Planetary Science Letters 279, 362-372.

Tsai, H.M., Meyer, H.O.A., Moreau, J., Milledge, H.J., 1979. Mineral inclusions in diamond: Premier, Jagersfontein and Finsch kimberlites, South Africa, and Williamson Mine, Tanzania, in: Meyer, H.O.A., Boyd, F.R., (Eds.), Proceedings of the 2nd International Kimberlite Conference. Geophysical Monograph, American Geophysical Union 1, 16-26.

Tukey, J.W., 1962. The Future of Data Analysis. Annals of Mathematical Statistics 33, 1-67.

Viljoen, K.S., Lawless, P.J., 1988. Finsch Mine—the largest diamond producer in South Africa. Geo bulletin—Quarterly News Bulletin of the Geological Society of South Africa 31, 48-49.

Weiss, Y., Kessel, R., Griffin, W.L., Kiflawi, I., Klein-BenDavid, O., Bell, D.R., Harris, J.W., Navon, O., 2009. A new model for the evolution of diamond-forming fluids: Evidence from microinclusion-bearing diamonds from Kankan, Guinea. Lithos 112, 660-674.

Weiss, Y., Kiflawi, I, Navon, O., 2010. IR spectroscopy: Quantitative determination of the mineralogy and bulk composition of fluid microinclusions in diamonds. Chemical Geology 275, 26-34.

Weiss, Y., Griffin, W.L., Bell, D.R., Navon, O., 2011. High-Mg carbonatitic melts in diamonds, kimberlites and the subcontinental lithosphere. Earth and Planetary Science Letters 309, 337-347.

Weiss, Y., Griffin, W.L., Navon, O., 2013. Diamond-forming fluids in fibrous diamonds: The trace-element perspective. Earth and Planetary Science Letters 376, 110-125.

Weiss, Y., McNeill, J., Pearson, D.G., Nowell, G.M., Ottley, C.J., 2015. Highly saline fluids from a subducting slab as the source for fluid-rich diamonds. Nature 524, 339-342.

Wilson, A.H., Shirey, S.B., Carlson, R.W., 2003. Archaean ultra-depleted komatiites formed by hydrous melting of cratonic mantle. Nature 423, 858–861.

Zedgenizov, D.A., Rege, S., Griffin, W.L., Kagi, H., Shatsky, V.S., 2007. Compositional variations of micro-inclusions in fluidbearing diamonds from Udachnaya kimberlite pipe as revealed by LA-ICP-MS. Chemical Geology 240, 151–162.

Zedgenizov, D.A., Ragozin, A.L., Shatsky, V.S., Araujo, D., Griffin, W.L., Kagi, H., 2009. Mg and Fe-rich carbonate-silicate high-density fluids in cuboid diamonds from the Internationalnaya kimberlite pipe (Yakutia). Lithos 112, 638-647.

Figure 1: Median double-normalized (chondrite-normalised (McDonough and Sun, 1995)) multiplied with $1/Er_N$) multi-element patterns of diamonds from Victor (Canada; sulphide and silicate paragenesis) for all acquired data, only for data above the LOD (limit of detection) and only for data above the LOQ (limit of quantification).

Figure 2: Double normalized (primitive mantle (McDonough and Sun, 1995) multiplied with $1/Er_N$) median and range of trace element concentrations in A. high-purity gem diamonds from Victor (black and red), and B. near-gem diamonds from Newlands (orange) and Finsch (blue). For Victor, the sulphide (black) and silicate (red) paragenesis analyzed in this study are defined by observed inclusion type. The range includes all data above the 25% and below the 75% quartile. Where no data points are present the lines are interpolated.

Figure 3: Double normalized (chondrite-normalized (N) (McDonough and Sun, 1995) multiplied with $1/Er_N$) median and range of rare earth element concentrations in A. high-purity gem diamonds from Victor (black and red), and B. near-gem diamonds from Newlands (orange) and Finsch (blue). For Victor, the

sulphide (black) and silicate (red) paragenesis analyzed in this study are defined by observed inclusion type. The range includes all data above the 25% and below the 75% quartile. Where no data points are present the lines are interpolated.

Figure 4: Box and whisker plots of primitive mantle-normalised La/Yb, Ba/Nb and Sm/Hf for high-purity gem diamonds from Victor (sulphide and silicate paragenesis) and near-gem diamonds from S. Africa (Newlands and Finsch). Ratios include all acquired data. The ends of the box are the upper (UQ) and lower (LQ) quartiles, so the box spans the interquartile range (IQR; the upper quartile minus the lower quartile). The median is marked by the vertical line inside the box. The whiskers are the two lines outside the box that extend to the highest and lowest observations. Disconnected points are potential outliers with values greater than UQ + 1.5 * IQR.

Figure 5: A. Chondrite-normalized (McDonough and Sun, 1995) REE concentrations for the two "end-member" patterns - 'planed' and 'ribbed' - of carbonatitic HDFs in fibrous diamonds (Weiss et al., 2013) and median REE concentrations for fibrous diamonds bearing saline HDFs from Ekati, Canada (Weiss et al., 2015). B. Median double normalized (chondrite-normalized (N) (McDonough and Sun, 1995) multiplied with $1/Er_N$) REE concentrations for the Victor high-purity gem diamonds (sulphide and silicate paragenesis) analyzed in this study and the Newlands and Finsch near-gem diamonds reported in this study.

Figure 6: Double-normalised multi-element (PM-Er) (A) and REE (C1-Er) (B) patterns for the range and medians of high-purity gem diamonds from Victor, Canada (sulphide and silicate paragenesis: this study) and high-purity gem diamonds from the Cullinan mine, S. Africa (McNeill et al., 2009). Ranges include all data above the 25% and below the 75% quartile. Where no data points are present the lines are interpolated.

Figure 7: Double-normalised trace element patterns for high-purity gem and near gem-quality diamonds from Victor (Canada; sulphide and silicate paragenesis) and South Africa (Cullinan, Newlands and

Finsch) (this study and McNeill et al., 2009), and for two "end-member" patterns, 'planed' and 'ribbed' that characterize the HDFs in fibrous diamond (Weiss et al., 2013). Data are normalised to primitive mantle and multiplied with $1/Er_N$ to equalise variations in abundance levels caused largely by differences in fluid inclusion abundance. Where no data points are present the lines are interpolated.

Figure 8: Primitive mantle-normalised diamond fluid trace element ratios in fibrous diamonds: (A) Ba/Nb vs La/Nb and (B) Th/Nb vs Nd/Nb (after Klein-BenDavid et al., 2014). Data from Klein-BenDavid et al., 2010, 2014; Weiss et al., 2013, 2015 and Smith et al., 2012. Also plotted are double-normalized (primitive mantle-normalized (N) (McDonough and Sun, 1995) multiplied with $1/Er_N$) median ratios for high-purity gem and near-gem diamonds from Victor (Canada), and from S. Africa (Cullinan, Newlands and Finsch) (this study and McNeill et al., 2009). The orange field is for saline HDFs, the yellow field for high Mg carbonatitic HDFs and the purple field for Low Mg carbonatitic – silicic HDFs. Legend: LMCS – Low Mg carbonatitic – silicic, HMC - high Mg carbonatitic.

Figure 9: Double-normalized (primitive mantle-normalized (N) (McDonough and Sun, 1995) multiplied with $1/Er_N$) median multi-element concentrations for near-gem diamonds from Finsch (this study) and fibrous diamonds containing saline HDFs, as established by major element analyses (Smith et al., 2012; Weiss et al., 2015).

Figure A1: Box and whisker plots of siderophile element concentrations in the Victor high-purity gem diamonds (sulphide and silicate paragenesis) analyzed in this study. The plots include all acquired data. The ends of the box are the upper (UQ) and lower (LQ) quartiles, so the box spans the interquartile range (IQR; the upper quartile minus the lower quartile). The median is marked by the vertical line inside the box. The whiskers are the two lines outside the box that extend to the highest and lowest observations. Disconnected points are potential outliers with values either greater than UQ + 1.5 * IQR or less than LQ – 1.5 * IQR.

Figure A2: Primitive mantle-normalized (McDonough and Sun, 1995) trace element concentrations in the sulphide bearing Victor diamonds analyzed in this study. Data in this plot is > LOQ. Samples V2-01 (square) and sample V2- V2-07 (triangle) show highly fractionated multi-element patterns that are characterised by positive Ce and Cs anomalies.

Figure A3: A. Primitive-mantle normalized (McDonough and Sun, 1995) trace element concentrations and B. chondrite normalized (McDonough and Sun, 1995) rare earth element concentrations of fluids in the xenolith derived near-gem diamonds from the Newlands and Finsch kimberlites analysed in this study.

Figure A4: A. Primitive-mantle normalized (McDonough and Sun, 1995) trace element concentrations and B. chondrite normalized (McDonough and Sun, 1995) rare earth element concentrations of fluids in the diamonds from the Cullinan mine (Data from McNeill et al., 2009). Diamond fluid with black lines are peridotitic, coloured lines are eclogitic.

Figure A5: Double-normalized (primitive mantle-normalized (N) (McDonough and Sun, 1995) multiplied with $1/Er_N$) multi-element patterns for near-gem diamonds from Finsch (S.Africa, this study) and cloudy and fibrous diamonds bearing saline HDFs from Canada (Diavik, Wawa and Ekati: Klein-BenDavid et al., 2014; Smith et al., 2012; Weiss et al., 2015) and Finsch, South Africa (Weiss and Goldstein, 2018).

Table 1: Provenance, host lithology, formation age and inclusion paragenesis of the fluids in the analyzed diamonds and those used for comparisons. *References for formation ages: Victor (Aulbach et al., 2018), Cullinan E-type (Richardson, 1986, Burgess et al. 1989, Phillips et al. 1989) Cullinan P-type (Richardson et al., 1993), Udachnaya, P-type ~ 3.1 - 3.5 Ga; Pearson et al., 1999), Finsch (Richardson et al., 1984) and Newlands (Menzies et al., 2003).

Name	Provenance	host lithology	Age	Inclusion		
V3-01	Victor, Superior Craton, Canada	P-type	~ 718 Ma	Garnet		
V3-03	Victor, Superior Craton, Canada	P-type	~ 718 Ma	Garnet		
V3-05	Victor, Superior Craton, Canada	P-type	~ 718 Ma	Garnet		
V3-11	Victor, Superior Craton, Canada	P-type	~ 718 Ma	Garnet		
A578-01	Victor, Superior Craton, Canada	P-type	~ 718 Ma	Garnet		
A578-02	Victor, Superior Craton, Canada	P-type	~ 718 Ma	Garnet		
A578-03	Victor, Superior Craton, Canada	P-type	~ 718 Ma	Garnet		
A578-04	Victor, Superior Craton, Canada	P-type	~ 718 Ma	Garnet		

V2-01	Victor, Superior Craton, Canada	P-type	~ 718 Ma	Sulphide		
V2-02	Victor, Superior Craton, Canada	P-type	~ 718 Ma	Sulphide		
V2-03	Victor, Superior Craton, Canada	P-type	~ 718 Ma	Sulphide		
V2-04	Victor, Superior Craton, Canada	P-type	~ 718 Ma	Sulphide		
V2-06	Victor, Superior Craton, Canada	P-type	~ 718 Ma	Sulphide		
V2-07	Victor, Superior Craton, Canada	P-type	~ 718 Ma	Sulphide		
V2-09	Victor, Superior Craton, Canada	P-type	~ 718 Ma	Sulphide		
V2-10	Victor, Superior Craton, Canada	P-type	~ 718 Ma	Sulphide		
New 01	Newlands, Kaapvaal craton, South Africa	E-type	~2.9 Ga	unknown		
New 02	Newlands, Kaapvaal craton, South Africa	E-type	~2.9 Ga	unknown		
New 03	Newlands, Kaapvaal craton, South Africa	E-type	~2.9 Ga	unknown		
New 04	Newlands, Kaapvaal craton, South Africa	E-type	~2.9 Ga	unknown		
f866 1	Finsch, Kaapvaal craton, South Africa	P-type (h)	~3.2 Ga	unknown		
f866 2	Finsch, Kaapvaal craton, South Africa	P-type (h)	~3.2 Ga	unknown		
jjg 1	Finsch, Kaapvaal craton, South Africa	P-type (h)	~3.2 Ga	unknown		
jjg 2	Finsch, Kaapvaal craton, South Africa	P-type (h)	~3.2 Ga	unknown		
Published Gem diamonds used for comparison						
AP25	Cullinan, Kaapvaal craton, South Africa	E-type	~2 Ga, ~ 1.2 Ga	Silicate		McNeill et al. (2009)
AP26	Cullinan, Kaapvaal craton, South Africa	E-type	~2 Ga, ~ 1.2 Ga	Silicate		McNeill et al. (2009)
AP28	Cullinan, Kaapvaal craton, South Africa	P-type (h)	~2 Ga	Silicate		McNeill et al. (2009)
AP30	Cullinan, Kaapvaal craton, South Africa	P-type (l)	~2 Ga	Silicate		McNeill et al. (2009)
AP31	Cullinan, Kaapvaal craton, South Africa	E-type	~2 Ga, ~ 1.2 Ga	Silicate		McNeill et al. (2009)
AP34	Cullinan, Kaapvaal craton, South Africa	E-type	~2 Ga, ~ 1.2 Ga	Silicate		McNeill et al. (2009)
AP35	Cullinan, Kaapvaal craton, South Africa	E-type	~2 Ga, ~ 1.2 Ga	Silicate		McNeill et al. (2009)
AP36	Cullinan, Kaapvaal craton, South Africa	E-type	~2 Ga, ~ 1.2 Ga	Silicate		McNeill et al. (2009)
AP37	Cullinan, Kaapvaal craton, South Africa	E-type	~2 Ga, ~ 1.2 Ga	Silicate		McNeill et al. (2009)
AP38	Cullinan, Kaapvaal craton, South Africa	E-type	~2 Ga, ~ 1.2 Ga	Silicate		McNeill et al. (2009)

Highlights

- It is now possible to obtain quantitative trace element data for gem diamonds
- Trace elements in Victor diamonds show subtle differences based on inclusion paragenesis
- Trace element patterns of gem diamonds are similar to those in fibrous diamonds
- •Very small highly dispersed fluid inclusions are measured in gem diamonds
- Finsch diamonds contain saline fluids, thought to originate from subducting slabs
- Parental fluids in both gem and fibrous diamonds have a common origin

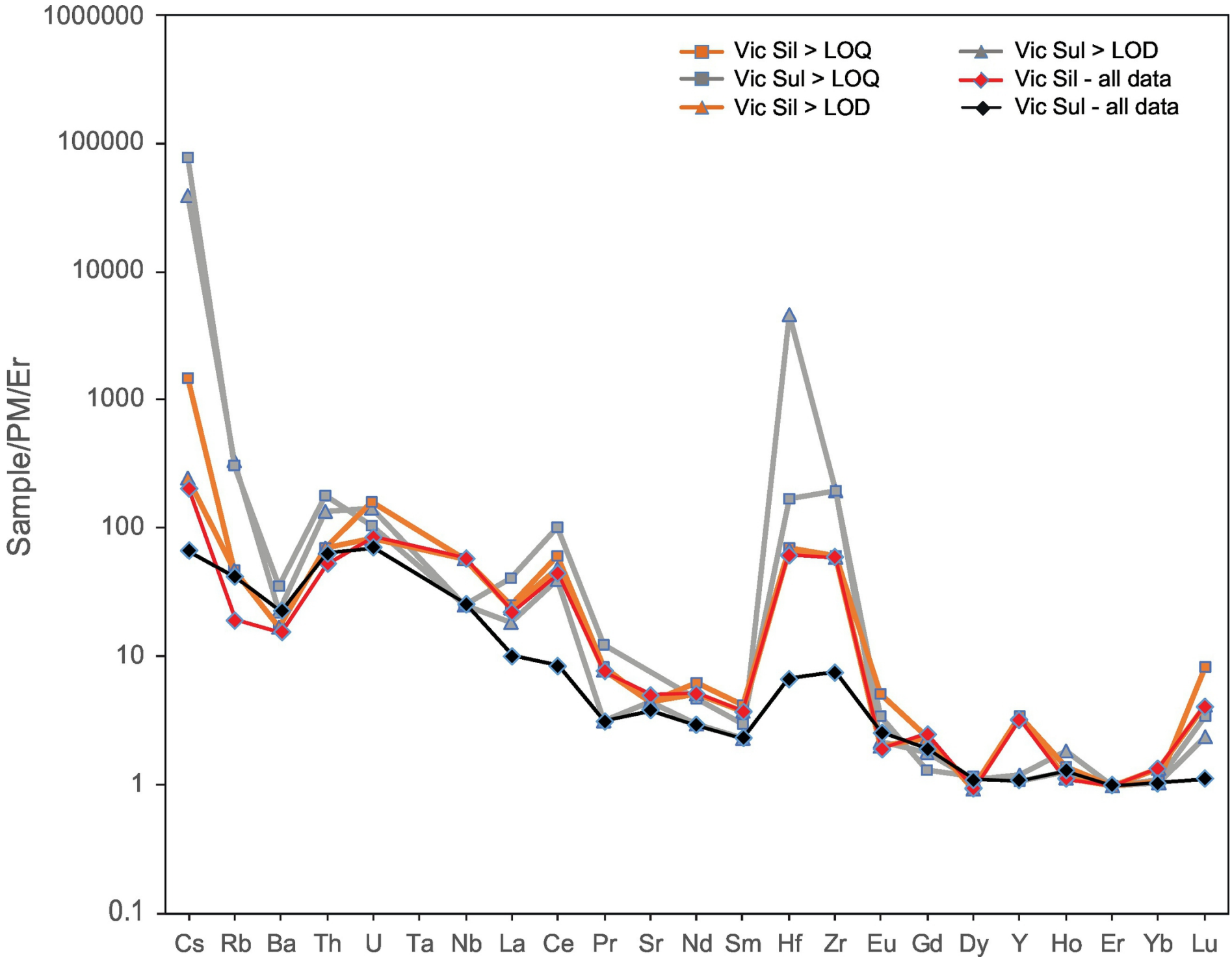
Vic Sil > LOQ
Vic Sul > LOQ
Vic Sil > LOD
Vic Sul > LOD
Vic Sil - all data
Vic Sul - all data
Sample/PM/Er
1000000
100000
10000
1000
100
10
1
0.1
Cs Rb Ba Th U Ta Nb La Ce Pr Sr Nd Sm Hf Zr Eu Gd Dy Y Ho Er Yb Lu

Figure 1

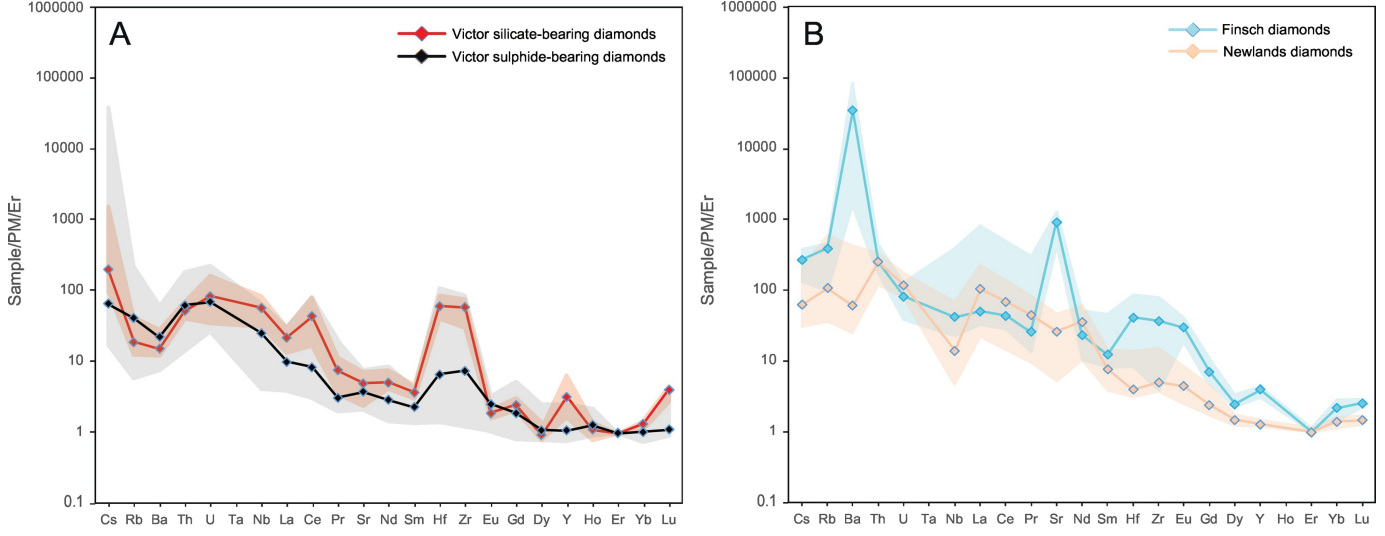
A
Victor silicate-bearing diamonds
Victor sulphide-bearing diamonds
Sample/PM/Er
1000000
100000
10000
1000
100
10
1
0.1
Cs Rb Ba Th U Ta Nb La Ce Pr Sr Nd Sm Hf Zr Eu Gd Dy Y Ho Er Yb Lu
B
Finsch diamonds
Newlands diamonds
Sample/PM/Er
1000000
100000
10000
1000
100
10
1
0.1
Cs Rb Ba Th U Ta Nb La Ce Pr Sr Nd Sm Hf Zr Eu Gd Dy Y Ho Er Yb Lu

Figure 2

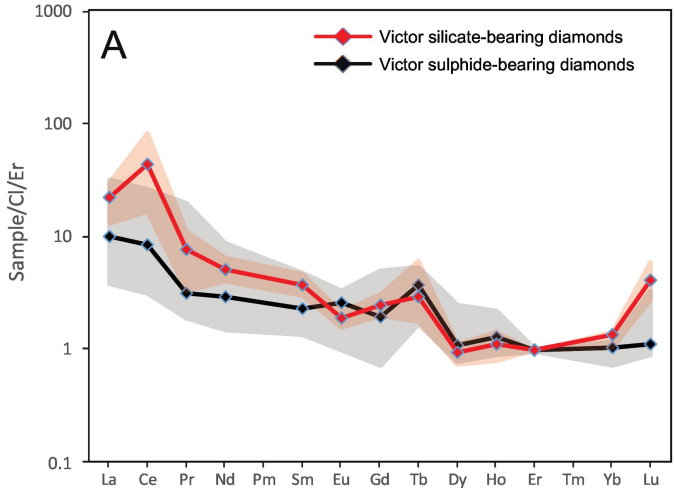
A
Victor silicate-bearing diamonds
Victor sulphide-bearing diamonds
Sample/Cl/Er
1000
100
10
1
0.1
La Ce Pr Nd Pm Sm Eu Gd Tb Dy Ho Er Tm Yb Lu

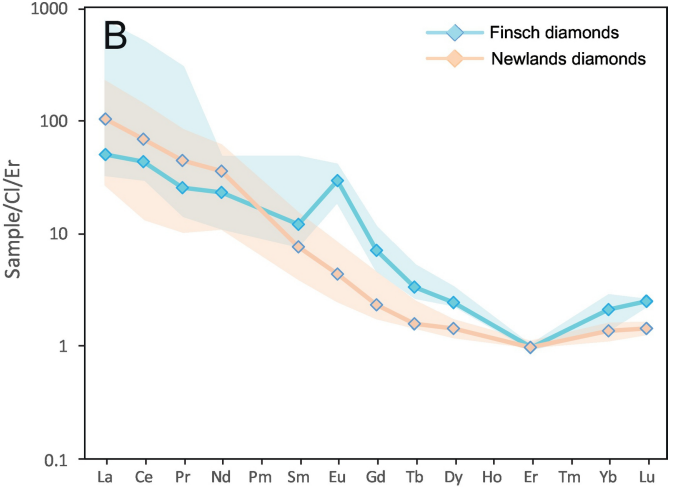
B
Finsch diamonds
Newlands diamonds
Sample/Cl/Er
1000
100
10
1
0.1
La Ce Pr Nd Pm Sm Eu Gd Tb Dy Ho Er Tm Yb Lu

Figure 3

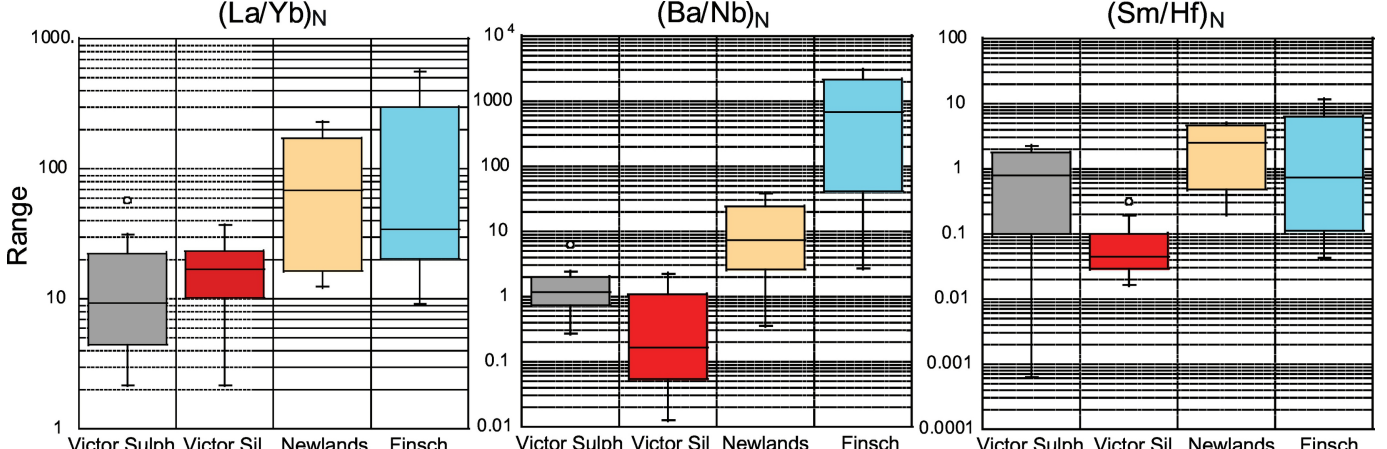
(La/Yb)N
(Ba/Nb)N
(Sm/Hf)N
Range
1000.
100
10
1
10 4
1000
100
10
1
0.1
0.01
100
10
1
0.1
0.01
0.001
0.0001
Victor Sulph
Victor Sil
Newlands
Finsch

Figure 4

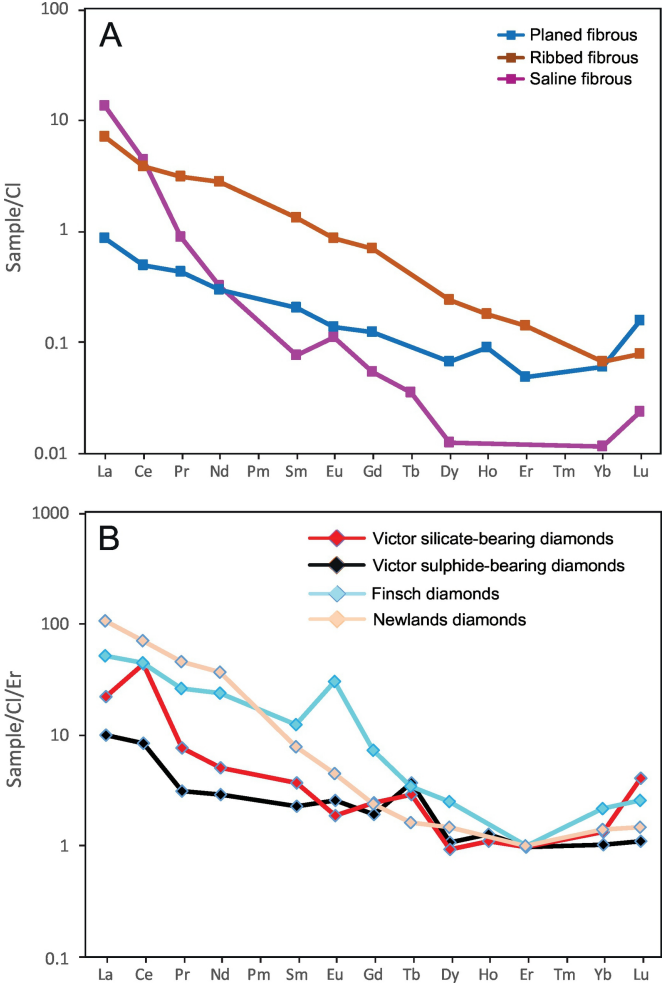
A
Planed fibrous
Ribbed fibrous
Saline fibrous
Sample/Cl
100
10
1
0.1
0.01
La Ce Pr Nd Pm Sm Eu Gd Tb Dy Ho Er Tm Yb Lu
B
Victor silicate-bearing diamonds
Victor sulphide-bearing diamonds
Finsch diamonds
Newlands diamonds
Sample/Cl/Er
1000
100
10
1
0.1
La Ce Pr Nd Pm Sm Eu Gd Tb Dy Ho Er Tm Yb Lu

Figure 5

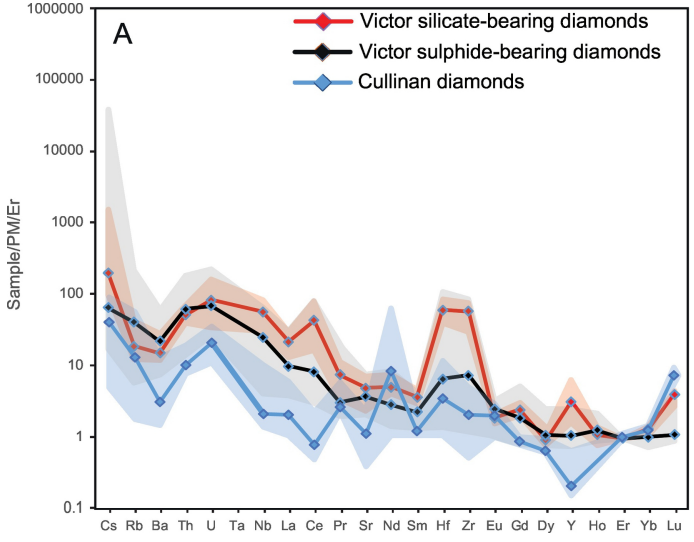
A
Victor silicate-bearing diamonds
Victor sulphide-bearing diamonds
Cullinan diamonds
Sample/PM/Er
1000000
100000
10000
1000
100
10
1
0.1
Cs Rb Ba Th U Ta Nb La Ce Pr Sr Nd Sm Hf Zr Eu Gd Dy Y Ho Er Yb Lu

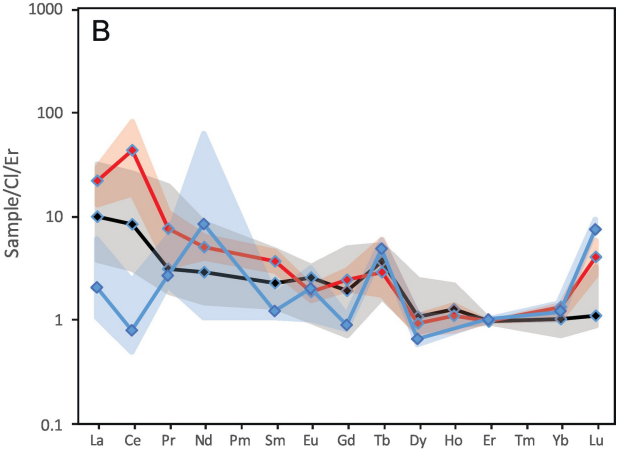
B
Sample/CI/Er
1000
100
10
1
0.1
La Ce Pr Nd Pm Sm Eu Gd Tb Dy Ho Er Tm Yb Lu

Figure 6

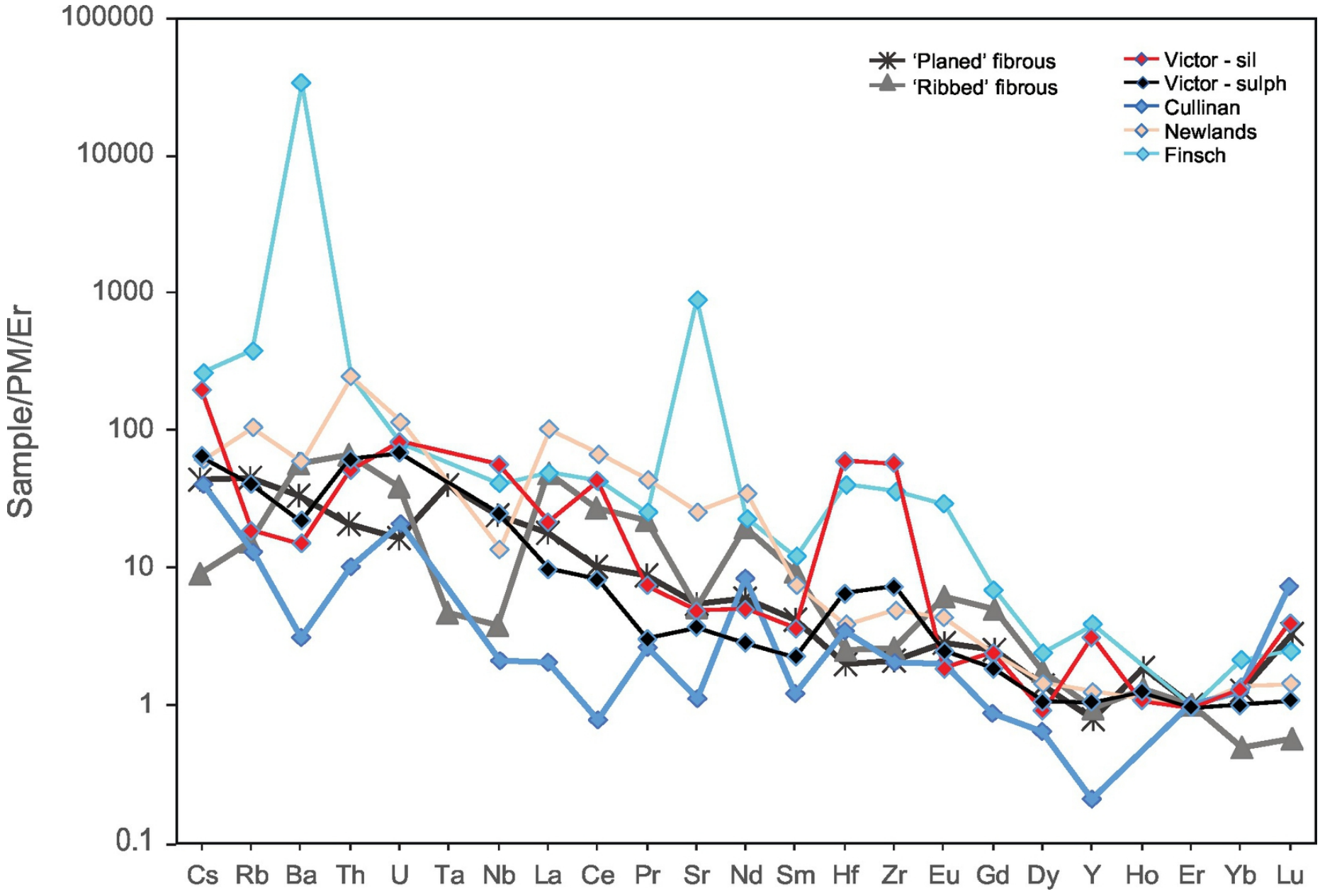
100000
10000
1000
100
10
1
0.1
Sample/PM/Er
'Planed' fibrous
'Ribbed' fibrous
Victor - sil
Victor - sulph
Cullinan
Newlands
Finsch
Cs Rb Ba Th U Ta Nb La Ce Pr Sr Nd Sm Hf Zr Eu Gd Dy Y Ho Er Yb Lu

Figure 7

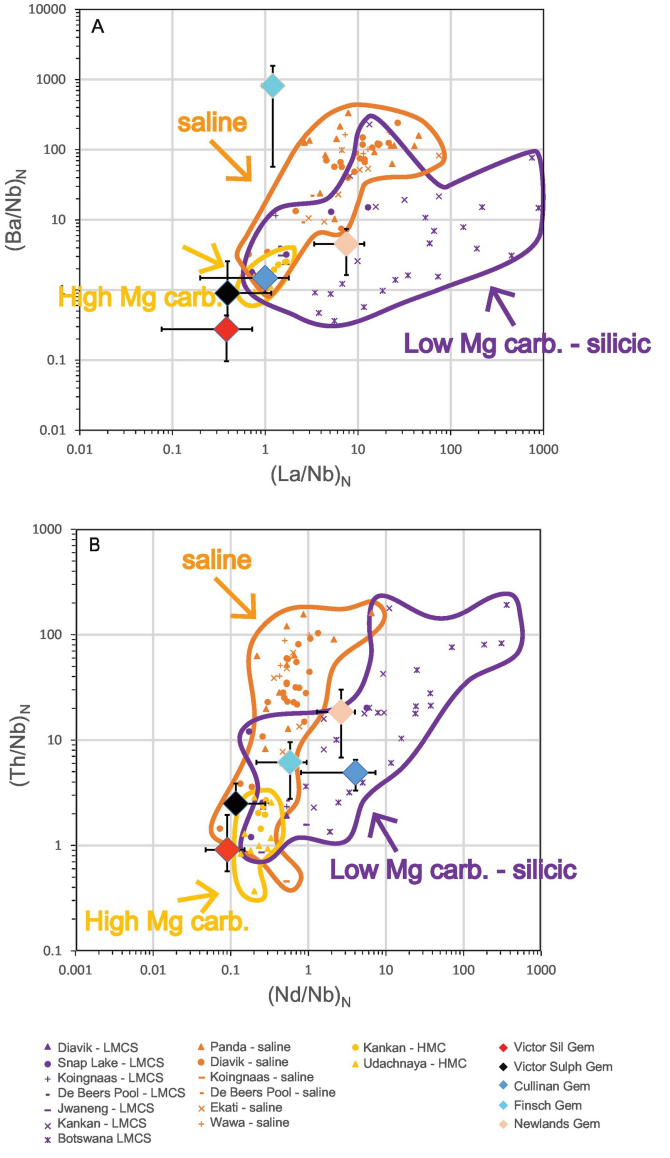
A
saline
High Mg carb.
Low Mg carb. - silicic
(Ba/Nb)N
(La/Nb)N
10000
1000
100
10
1
0.1
0.01
0.01
0.1
1
10
100
1000
B
saline
Low Mg carb. - silicic
High Mg carb.
(Th/Nb)N
(Nd/Nb)N
1000
100
10
1
0.1
0.001
0.01
0.1
1
10
100
1000
Diavik - LMCS
Snap Lake - LMCS
Koingnaas - LMCS
De Beers Pool - LMCS
Jwaneng - LMCS
Kankan - LMCS
Botswana LMCS
Panda - saline
Diavik - saline
Koingnaas - saline
De Beers Pool - saline
Ekati - saline
Wawa - saline
Kankan - HMC
Udachnaya - HMC
Victor Sil Gem
Victor Sulph Gem
Cullinan Gem
Finsch Gem
Newlands Gem

Figure 8

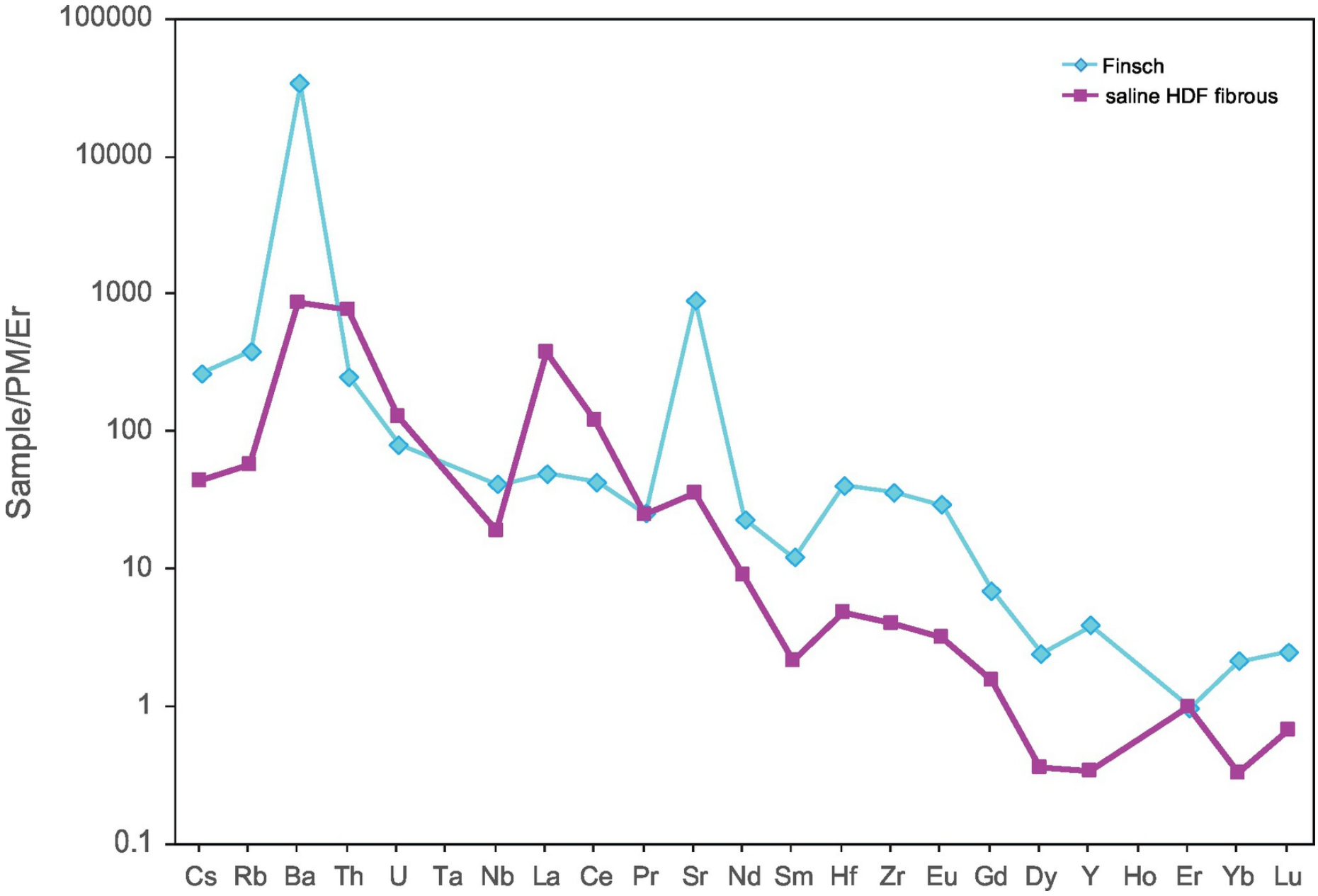
Finsch
saline HDF fibrous
Sample/PM/Er
100000
10000
1000
100
10
1
0.1
Cs Rb Ba Th U Ta Nb La Ce Pr Sr Nd Sm Hf Zr Eu Gd Dy Y Ho Er Yb Lu

Figure 9